# Microlidar observations of biomass burning aerosol over Djougou (Benin) during African Monsoon Multidisciplinary Analysis Special Observation Period 0: Dust and Biomass-Burning Experiment

Jacques Pelon, Marc Mallet, A. Mariscal, P. Goloub, Didier Tanré, Diana Bou Karam, Cyrille Flamant, J. Haywood, B. Pospichal, S. Victori

# Microlidar observations of biomass burning aerosol over Djougou (Benin) during African Monsoon Multidisciplinary Analysis Special Observation Period 0: Dust and Biomass-Burning Experiment

J. Pelon,[1] M. Mallet,[2] A. Mariscal,[2] P. Goloub,[3] D. Tanré,[3] D. Bou Karam,[1] C. Flamant,[1] J. Haywood,[4] B. Pospichal,[5] and S. Victori[6]

Received 18 February 2008; revised 28 April 2008; accepted 18 June 2008; published 13 December 2008.

[1] Microlidar observations have been performed at the Djougou-Nangatchori site in northern Benin during the African Monsoon Multidisciplinary Analysis (AMMA) Special Observation Period 0 in the dry season, combined with the Dust and Biomass-Burning Experiment (DABEX) from mid-January to mid-February 2006. During the dry season, the Djougou area is a region where biomass burning aerosols are heavily produced from agriculture fires. The aerosol vertical distribution is also controlled by dynamics, and the penetration of the winter monsoon flux to the north and northern winds bringing mineral dust to the South leads to a frontal discontinuity location close to Djougou latitude. During the early dry season, the aerosol vertical distribution was observed to be structured in two layers, the lower being the boundary layer reaching altitudes up to 2 km and the upper one corresponding to the trade wind layer extending up to 5 km. Lidar data are used to retrieve the time evolution and vertical profile of extinction and discuss transport processes during the period analyzed. As the monsoon flux during the dry season is steadily progressing to the north but also moving back and forth according to shorter timescale forcings, biomass burning particles are transported from the boundary layer into the upper troposphere. This transport has a strong impact on the distribution of aerosol particles on the vertical, and extinction values larger than 0.3 $km^{-1}$ have been retrieved at altitudes close to 3 km. A particular event of biomass burning air mass outbreak associated with a synoptic forcing is studied, where satellite observations are used to discuss observations of biomass burning particles over Djougou and at the regional scale.

**Citation:** Pelon, J., M. Mallet, A. Mariscal, P. Goloub, D. Tanré, D. Bou Karam, C. Flamant, J. Haywood, B. Pospichal, and S. Victori (2008), Microlidar observations of biomass burning aerosol over Djougou (Benin) during African Monsoon Multidisciplinary Analysis Special Observation Period 0: Dust and Biomass-Burning Experiment, *J. Geophys. Res.*, *113*, D00C18, doi:10.1029/2008JD009976.

## 1. Introduction

[2] The African continent is the largest global source of both mineral dust aerosols [*Prospero et al.*, 2002] and biomass burning aerosols [*Andreae and Merlet*, 2001]. These aerosols are known to significantly affect the solar and terrestrial radiation thereby modifying the incoming and outgoing shortwave and longwave radiations. In the case of aerosol transport over the ocean, as observed during the dry monsoon season over Indian Ocean [*Pelon et al.*, 2002], they can significantly reduce the radiation flux available at the surface, thereby modulating its energy budget. The determination of aerosol optical depth (AOD) is of critical importance to these studies. In addition to that, these aerosols absorb a significant proportion of both solar and terrestrial radiation in the atmospheric column. It has been shown that absorption of solar radiation by such aerosols may have a significant impact on the sign of the TOA direct radiative forcing, which may change, depending of the surface albedo [*Fraser and Kaufman*, 1985]. Furthermore, due to their significant optical depths over Africa, dust and biomass air masses strongly modify the heating rates of the atmosphere, depending to their vertical distribution. Mixing and, further on, aging, sedimentation, and cloud processing occurring over land and ocean will then result in a variable forcing which needs to be better understood. This is the purpose of the AMMA SOP0/DABEX field experiment (J. M. Haywood et al., Overview of the Dust and Biomass Burning Experiment and African Monsoon Multidisciplinary Analysis Special Observing Period-0, submitted to *Journal of Geophysical Research*, 2008).

[3] Dust storms over West Africa frequently occur during spring and summer months of the Northern Hemisphere

[1]SA, IPSL, CNRS, Universite Pierre et Marie Curie, Paris, France.
[2]LA, UPS, CNRS, Toulouse, France.
[3]LOA, Université Lille 1, CNRS, Villeneuve d'Asq, France.
[4]Met Office, Exeter, UK.
[5]Institute for Geophysics and Meteorology, University of Cologne, Cologne, Germany.
[6]CIMEL Electronique, Paris, France.


0148-0227/08/2008JD009976

(February to August) [*d'Almeida*, 1986], mostly linked to meteorological synoptic situations leading to strong northerly flows [*Tulet et al.*, 2008]. Several measurement campaigns have however focused on studying dust aerosols during the summer months [*Karyampudi et al.*, 1999; *Tanré et al.*, 2003; *Berthier et al.*, 2006]. Such campaigns took advantage of lidar observations for the identification and characterization of the structure of aerosol layers. Biomass burning aerosols have been extensively characterized during the SAFARI campaign held in southern Africa (Namibia) during the dry season [*Haywood et al.*, 2003]. This has not been the case for such aerosols produced during the dry season in western Africa.

[4] Satellite remote sensing has been used for long for the analysis of the AOD from visible-infrared sensors such as the Advanced Very High Resolution Radiometer (AVHRR) [*Husar et al.*, 1997] or the Total Ozone Mapping Spectrometer (TOMS) [*Prospero et al.*, 2002]. The launch of both Terra and Aqua satellites embarking the Moderate Resolution Imaging Spectroradiometer (MODIS) has further allowed a better characterization of aerosol types due to advanced analysis capabilities [*Remer et al.*, 2005]. Even if advances in analysis methods have been made, taking advantage of altitude selective absorption, passive instruments on board satellites do not allow an accurate characterization of absorbing aerosol on the vertical. New approaches have been proposed to combine lidar and radiometry, namely in the frame of the synergism offered by the AQUA-train [*Kaufman et al.*, 2003]. Using ground-based lidar, in combination with Aerosol Robotic Network (AERONET)/Photométrie pour le Traitement Opérationnel de Normalization Satellitaire (PHOTONS) observations is also of importance for this purpose, as it offers networking possibilities.

[5] In this paper, we present results on aerosol structural and optical properties on the vertical obtained during January and February 2006 in the frame of the SOP 0 (Special Observation Period 0), on the Djougou site (9.70°N/1.68°W, northern Benin), based on quasi-continuous microlidar observations. We present the instrumentation in section 2. Section 3 is dealing with the presentation of the context of the observations, both in terms of aerosol parameters and dynamics. Section 4 details the analysis method. Results are presented and discussed in section 5. We analyze in this section the observations in terms of transport and link ground-based observations to satellite ones for a particular event related to the northward outbreak of biomass burning particles. The impact on radiative budget is further discussed in another paper [*Mallet et al.*, 2008].

## 2. Instrumentation

[6] Djougou has been designed to be a supersite for ground-based instrumentation to characterize the microphysical and optical properties of expected mixed dust and biomass burning aerosols. Two other sites were more particularly equipped in the northern Sahel to document dust transport: Niamey-Banizoubou in Niger [*Heese and Wiegner*, 2008] and M'Bour in Senegal [*Derimian et al.*, 2008].

[7] During AMMA-SOP0/DABEX the Djougou site was equipped with in situ (nephelometer, aethalometer, aerosol particle counters) and remote sensing instruments (a CIMEL microlidar and radiometers), placed under responsibility of Laboratoire d'Aérologie [*Mallet et al.*, 2008]. A ceilometer, radar, and radiometer were installed by Universities of Köln and Bonn [*Pospichal and Crewell*, 2007]. Close to these instruments, an automated CIMEL Sun photometer was operated in the frame of AERONET (http://aeronet.gsfc.nasa.gov/) and its subpart PHOTONS (http://www-loa.univ-lille1.fr/photons).

[8] This setup was complemented by aircraft (BAe 146 from UKMO/NERC) and we used here data from the three-wavelength integrating nephelometer, TSI model 3563, operating at 450, 550, and 700 nm. The field experiment also involved an ultralight aircraft (LSCE/CNRS-CEA), as well as satellite observations, as described in the AMMA-SOP 0/DABEX preparation document (available at http://www.amma-international.org) (Haywood et al., submitted manuscript, 2008). The AMMA-SOP 0/DABEX started on 13 January and lasted until 16 February. The BAe 146 was based in Niamey (Niger) from January 13 to 2 February and then operated from Dakar, Senegal.

[9] The Cloud and Aerosol Microlidar (CAML) CE 370−2 is developed by the CIMEL company. This lidar is an eye-safe micropulse lidar system operating at $\lambda_{Ca}$ = 532 nm. Its characteristics are given in Table 1. The rack contains the laser source and the detection optics and electronics. Its principle is similar to the one of the micropulse lidar system that has been involved in previous field campaigns by U.S. groups [*Welton et al.*, 2002]. However, there are some differences in design that allow an easier operation, such as the telescope which was placed outside a small building, where all the acquisition systems were located. The main difference is the emission and reception optical link from the rack to the telescope (composed of a doublet lens), that is ensured by a 10 m optical fiber. This design reduces the full overlap distance with respect to a standard nonfibered design as laser beam emission is characterized by speckles, and the divergence at the fiber output is smaller than the numerical aperture. Signal detection and processing is ensured by an avalanche photodiode (Perkin-Elmer SPCM-AQR-12), protected by an acousto-optic device deviating the received beam during laser emission, a photon counting system (30 km range, at 15 m resolution) and a summation processor, both developed by Cimel. Owing to the acousto-optic system, no useful signal is detected from altitudes below 150 m. Files corresponding to profile averages over 1s are stored in the internal memory and are transferred to the external control computer. Measurements were made according to a standard sequence of 10 min acquisition every half hour. The IPSL/SA CAML system was installed in Djougou on 20 January and was operated during SOP 0 from 20 January to 13 February 2006.

## 3. Environmental and Meteorological Context

[10] During the dry season in Northern Hemisphere, fire sources in Africa are located in a latitudinal band spanning from the coast, close to 8°N up to 11°N. This is shown in Figure 1 for the month of January, as derived from MODIS observations by the Rapid Response System (http://rapidfire.

**Table 1.** Main Characteristics of the Microlidar System (Cloud and Aerosol Microlidar) Installed in Djougou

| Characteristic | Value |
|---|---|
| Rack size | standard 6U |
| Emitted energy | 8 $\mu$J |
| Pulse repetition rate | 4.7 kHz |
| Telescope size | 20 cm |
| Focal length | 0.90 m |
| Field of view | 100 $\mu$rd |
| Complete overlap range | 2.5 km |
| Maximum analysis range | 30 km |
| Range resolution | 15 m |
| Time resolution (individual files) | 1 s |

sci.gsfc.nasa.gov/). As seen in Figure 1 fire places (identified as red spots) leading to the production of biomass burning particles are very important in number over western Africa. They are also very dense in the region of the rural site of Djougou as reported in Figure 1. The number of fires is maximal in December–January and then decreases as a function of time, as given by MODIS observations. The total number of fires in the area between 20°W and 10°E is indeed decreasing not uniformly over the area during whole dry season. Fires in the western part are reactivated end of February, whereas the activity near Djougou is steadily decreasing until the end of February. It is to be noticed that over Djougou area, the fire activity slightly increases again in the beginning of March before vanishing.

[11] In Djougou biomass burning aerosol is expected to be the primary source of aerosols in the atmosphere, especially close to the maximum of the fire activity. These fires are linked to an agricultural practice, and rather small parcels are burnt at the same time. Fires are not very intense, and the particles produced are transported to altitudes of a few hundred meters by forced convection, as seen from aircraft observations [*Johnson et al.*, 2008]. Indeed, the Sun-heated surface induces a more important convection during daytime that leads to a large mixing of particles in the boundary layer, which top is reaching about 2 to 2.5 km, as derived from our measurements (see below). As seen from Figure 2, the average optical depth at 870 nm measured by Sun photometer is close to 0.5 on average, without any marked long-term trend, corresponding to the decrease of fire activity, but significant events are seen to occur that lead to enhanced AOD values. We have reported on the same figure the evolution of the Angström exponent $A$ (wavelength dependence of the AOD expressed as $\lambda^{-A}$), deduced from the wavelength variation of the AOD. One can see that a constant decrease is this time observed during the first 2 months. We also note (not shown) that at the beginning of March a large dust event was detected from satellite observations to transport a lot of dust over this area [*Tulet et al.*, 2008], for which the Angström exponent was close to 0, as expected for large particle sizes. It is seen that on the contrary, at the beginning of the observation period, this coefficient was maximal (close to 1.2). This value is consistent with the one obtained from aircraft data for upper air measurements [*Johnson et al.*, 2008]. Indeed, to a first order, the evolution of the Angström exponent, derived from Sun photometers, reflects the evolution of the size of the aerosol particles averaged in the column with a weighting function linked to the extinction coefficient profile in the column [*O'Neill et al.*, 2002]. This coefficient is close to 2 in the case of theoretical Mie calculations made for the small mode of the distribution of biomass burning particles measured by the BAe 146 [*Johnson et al.*, 2008]. This shows that even near the maximum of the fire activity, big particles are observed, most of which probably being mineral dust in the boundary layer. Further to the overall trend, we can notice in Figure 2 different peaks where the variations of AOD and Angström exponent are opposed in phase. This can be identified as mineral dust transport from northern latitudes. A more favorable period to observe these events appears to be at the end of February (14–22 February), which happened after the end of the SOP 0. It is however more difficult to identify in Figure 2 events for which the correlation between AOD and Angström exponent is strongly positive, with respect to the trend identified. One can see that the large increase in AOD observed after the 17 January is not linked to a strong decrease in the Angström exponent A, as it would be expected for dust transport, but rather to an increase in A. The period from 17 to 30 January is thus expected to be dominated by biomass particle production or advection. We will focus more particularly on the first part of this period,

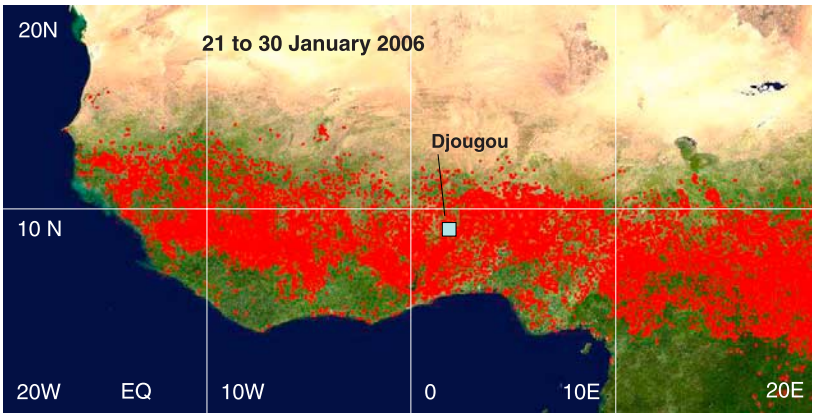


**Figure 1.** Fires sources identified by Moderate Resolution Imaging Spectroradiometer (MODIS) over West Africa during the period from 21 to 30 January 2006.

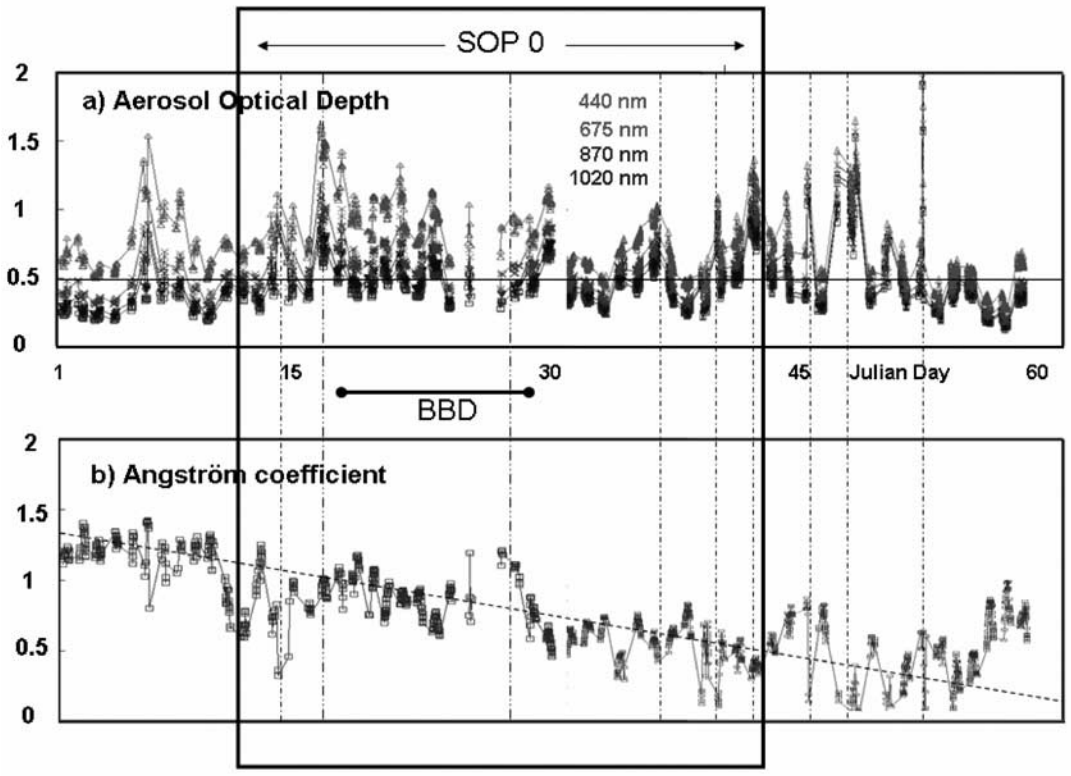


**Figure 2.** Aerosol Robotic Network (top) aerosol optical depth and (bottom) Angström exponent obtained at Djougou in January and February 2006. The rectangle delimits the Special Observation Period 0 duration, and the line marked "BBD" identifies the period where aerosol originating from biomass burning is expected to dominate in the aerosol optical depth.

extending from 17 to 24 January, which is labeled in Figure 2 as a biomass burning dominated (BBD) period.

[12] The circulation pattern during the dry season is a function of altitude, which may vary on a daily basis with the meteorological synoptic forcing. We have reported in Figure 3, the wind speed and streamlines at four different levels (surface, 850, 500, 300 hPa) for the 21 January 2006, from NCEP/NOAA analyses. At the surface, the wind

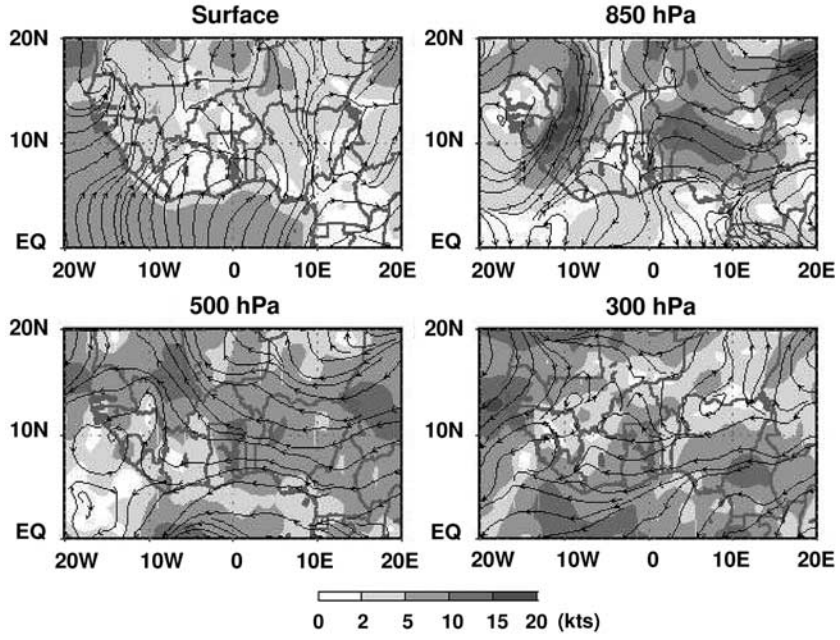


**Figure 3.** Wind speed (lower scale in knots) and direction at four pressure levels (surface, 850 hPa, 500 hPa, and 300 hPa) over West Africa for 21 January 2006, 0000 LT (NOAA-NCEP).

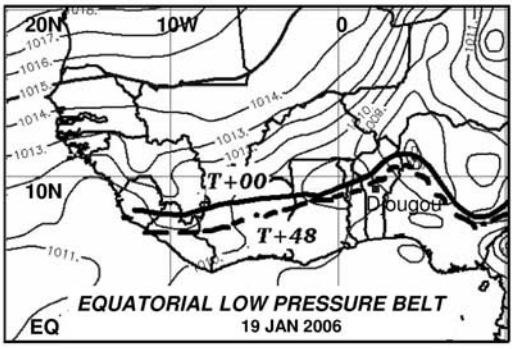


**Figure 4.** Surface pressure field and intertropical discontinuity (ITD) evolution during African Monsoon Multidisciplinary Analysis Special Observation Period 0: Dust and Biomass-Burning Experiment analysis for 19 January 2006 (from African Center of Meteorological Applications for Development Bulletin). Solid and dotted lines give the position of the ITD at 0000 UTC on 19 January and 48 h later, respectively.

blowing from the south is linked to the penetration flux of maritime air in a large scale synoptic flow, forced by differential land-ocean heating. The position of the head of this penetrative monsoon current, called the intertropical discontinuity (ITD), is controlled by the northern flux and the available energy of the current. It is marked by a strong gradient in moisture and wind. The inland progression of this moist air layer is linked to the evolution of forcings at different scales including the diurnal cycle [*Parker et al.*, 2005; *Ramel et al.*, 2006]. During the period of observations, its position was north to Djougou area, close to 11°N (see Figure 4) as derived from analyses of the African Center of Meteorological Applications for Development (ACMAD). It was observed to vary over the SOP 0. At latitudes north of Djougou, surface wind leads to a southward transport of mineral material in the advected boundary layer air masses. As discussed before, extinction due to mineral material presents a very small Angström exponent, and the smaller biomass burning particles can be identified by a larger Angström exponent close to 1. This is what we can see from measurements made with the three-wavelength TSI nephelometer on board the BAe 146, flying in the boundary layer north to south at a flight level of 500 feet (FL05, about 150 m above the surface) during mission B159 (19 January 2006), as reported in Figure 5. North of 10°N, which is close to the ITD position, the extinction coefficients measured show an Angström exponent close to 0, whereas in the south, getting in the fire region, this coefficient progressively increases. It is about 0.5 from the 550 to 700 nm ratio close to Djougou area at 150 m altitude, just before the ascent to 1500 m. Looking to the measurements at an altitude of 1500 m (FL50) it is closer to 1.

[13] The flux at 850 hPa west of Djougou is preferentially oriented from north to south (Figure 3). On 21 January, a northerly flow is observed in the area west of 5°W linked to a formation of a pressure low. An easterly flow (usual pattern) is observed east of this longitude. This pressure level appears as a transition level and the flux up to pressure level of 600 to 500 hPa (this level is marking the transition from the trade wind region to the free tropospheric flow) is oriented westerly at latitudes lower than 20°N. The subtropical jet (300 hPa) is located near 30°N on average, but during the period under analysis, significant perturbations were observed, as linked to a synoptic low-pressure system moving eastward over northern Africa. We then observed a pattern showing more northwesterly flows at low latitudes (close to 15°–20°N) and west of 10°W longitudes in the free troposphere (above 600 hPa). A southwesterly flow east of longitudes of 0°W, linked to a persisting through in altitude over northern Africa was present over the north of Djougou. This situation has an impact on the long range transport from the Sahel to northern latitudes and is expected to disturb the usual pattern of transport of aerosols, through the coupling of midlevel and upper-level flows.

## 4. Analysis Method

[14] Several steps are needed to derive backscatter and extinction profiles in the atmosphere using CAML system. We will hereafter detail the procedure which, close to the one previously developed for such microlidar observations [*Welton et al.*, 2002], was developed by our group for the analysis.

### 4.1. Vertical Structure

[15] During a 10 min data acquisition sequence, 10 individual profiles are acquired and averaged. Taking pre-

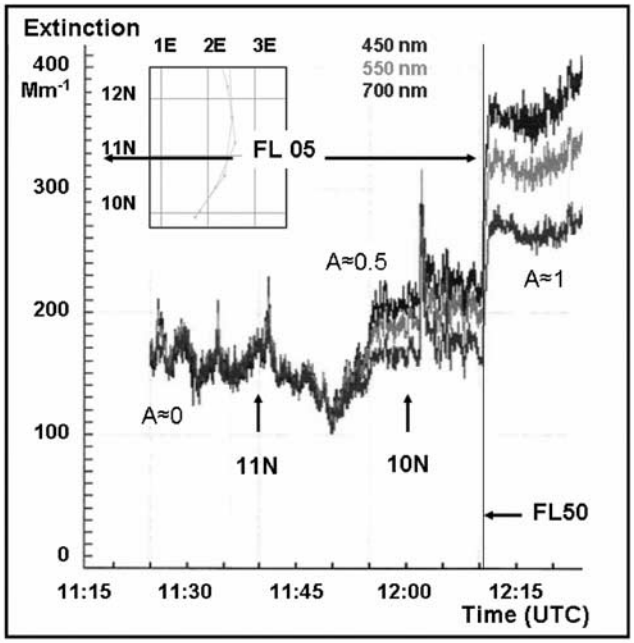


**Figure 5.** Variation of the extinction coefficient measured by the three wavelength nephelometer on board the U.K. Met Office BAe 146 during its transit from Niamey area to Djougou area (see included track) at 500 feet during mission B159 on 19 January 2006. A change in level to reach 5000 feet has been made at 1210 LT. An estimate of the Angström exponent observed is given. The final value A≈1 obtained at 5000 feet is comparable to the one given by the Sun photometer in Figure 2. indicative of a larger contribution of upper levels in the Sun photometer aerosol optical depth (AOD).

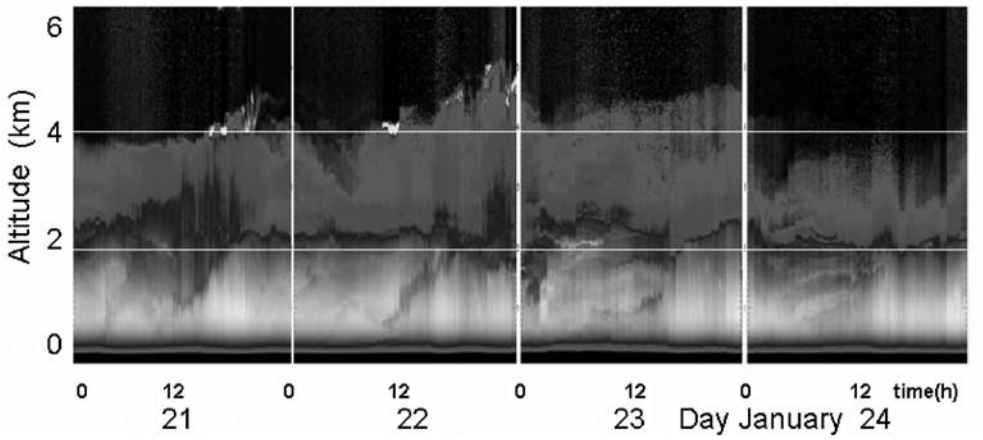


**Figure 6.** Evolution of the lidar signal for the period from 21 January to 24 January 2006. The black curves underline the maximum of gradient in the vertical aerosol profile linked to the development of the daytime boundary layer.

vious analyses into account [*Dupont et al.*, 1994; *Flamant and Pelon*, 1996; *Menut et al.*, 1999], the lidar profiles allow to derive the altitude of the structural parameters (boundary layer height and upper inversion height) as well as optical parameters (extinction profile and lidar ratio).

[16] From the profiles obtained every 30 min one can materialize the evolution of the boundary layer. Figure 6 presents the series of observations made from 21 January to 24 January 2006. The evolution of the boundary layer height is given by the black line. At 1200 local time (LT), it is close to 1 km and continues to grow until sunset (19 h LT), up to 2 km. The modulation of the BL height (BLH) appears to be small on a day-to-day basis even if the rate of change of the BLH is different. The aerosol load is observed to decrease only above an altitude of 4 to 5 km marking the top of the trade wind layer. Some clouds are observed on 21 and 22 January at this altitude.

[17] As a side product, it can be noticed that the growth of the boundary layer height is linked to the net heating rate Q in the BL taking into account the entrainment at the top and radiation heating due to absorption by aerosols. To a first approximation, the growth rate of the BL height, *h*, can be derived from the knowledge of the gradient of the signal as previously obtained by *Dupont et al.* [1994] BL growth is materialized by solid lines reported in Figure 6. Knowing the potential temperature gradient would allow to derive the total heating in the BL depending on entrainment dynamics [*Flamant and Pelon*, 1996]. The determination of the heating due to aerosol absorption then allows to retrieve surface sensible heat flux. This will be the object of further analyses.

### 4.2. Corrections on the Signal

[18] As the lidar system is based on the emission of low energy pulses to be eye-safe, the use of a high-efficiency photon counting device is needed. Furthermore, a narrow field of view is imperative to reject background daylight as much as possible for optimal daytime operation. This last constraint implies that a geometrical factor O(r) is introduced which reduces the received lidar signal as a function of range r. Considering the lidar equation, the detected lidar signal P(r) can be expressed as

$$P(r) = C\frac{O(r)}{r^2}\beta(r)T^2(r) \tag{1}$$

where C is a calibration constant and T(r) is the atmospheric transmission corresponding to the integrated extinction by aerosols along the observation path

$$T(r) = \exp - \int_0^r \alpha(r)dr.$$

The detector of the microlidar system is an avalanche photodiode operating in a photon counting mode. It is known to present a spurious signal (called afterpulse signal), larger in the first microseconds due to the detection of scattered laser light in the receiver at each emitted laser pulse [*Welton et al.*, 2002]. To correct this effect, the detected signal was recorded when the light emission was blocked at the telescope output. A reference signal was thus generated, which was averaged over a large number of shots (several sequences were averaged over several days). This afterpulse reference signal was substracted to all recorded profiles.

[19] As a second step, these profiles are normalized to molecular scattering in clear air above the upper inversion layer. One then obtain the vertical profiles of the attenuated backscattering coefficient (ABC), as reported in Figure 7a. This is corresponding to write ABC(r) instead of P(r), in equation (1) and using C = 1. It is then needed to correct the overlap factor so to extend the profile as close to the surface as possible [*Welton et al.*, 2002]. This has been done here using the slope method [*Kunz and de Leeuw*, 1993]. This method is assuming the atmosphere is perfectly mixed, which implies that the backscatter and extinction coefficients ($\beta$(r) and $\alpha$(r), respectively) are constant with range r in the atmosphere.

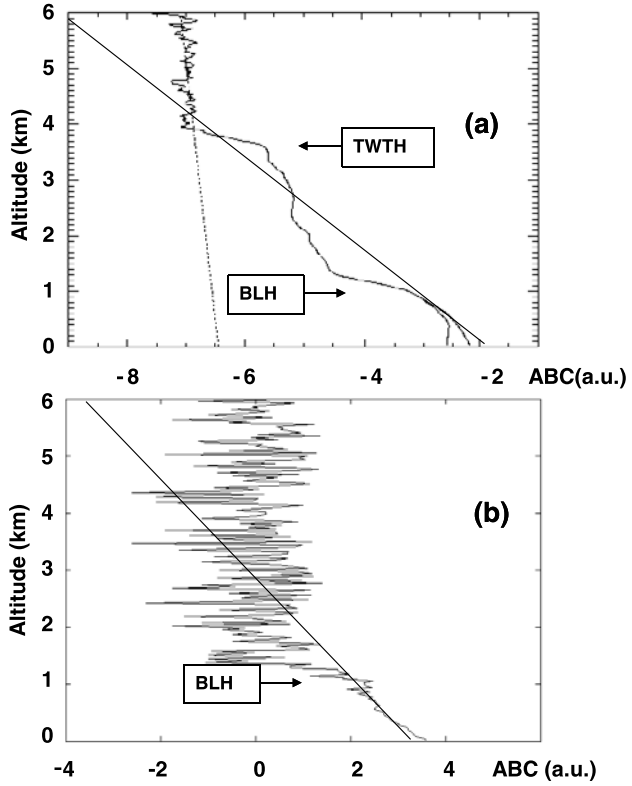


**Figure 7.** (a) Retrieved attenuated backscattering coefficient (ABC, solid line) in logarithmic scale (Ln(ABC) where ABC is in $km^{-1}$ $sr^{-1}$) as a function of altitude (10 min and 75 m resolution) for the 21 January near 1400 LT. Dotted line is molecular backscattering from the seasonal model used for normalization. The boundary layer height (BLH) and the trade wind layer top height (TWTH) identified as the altitudes with maximal gradients in the ABC are indicated. (b) Range corrected signal obtained with the CT25K ceilometer in logarithmic scale. BLH found from the gradient in ABC is also indicated. Solid lines represent the best fit to the backscattered signal in the boundary layer between 400 and 700 m. In both Figures 7a and 7b, the solid straight line has the slope of the ABC between 500 and 800 m in the boundary layer.

[20] The slope method assumes that O(r) = 1 in the full overlap region between emission and reception so that the logarithmic derivative of P(r) writes

$$\frac{dP}{Pdr}(r) = \frac{d\beta(r)}{\beta dr} - 2\alpha(r) \qquad (2)$$

but also that the backscatter coefficient is constant, so that it reduces to the extinction coefficient. Here we just need that the right-hand term is constant, so that this value can then be used in (1) to correct transmission and derive the O(r) profile as a function of range. In the boundary layer, at 532 nm, scattering by particles is much larger than scattering by molecules, and these coefficients can be considered as linked to particle scattering only. We have thus used horizontal observations made over several days and fitted a function normalized to 1 at long range to obtain O(r). This function was used as the initial overlap correction in the vertical profile analysis of all CAML data above 350 m. The signal was then extrapolated down to the surface keeping the same slope as the signal dP/dr just above. Figure 7a shows an example of the attenuated backscatter coefficient profile obtained on 21 January close to 1400 LT over 10 min acquisition. This corresponds to a developed BL during daytime, so that the aerosol distribution should be more homogeneous.

[21] As the correction remains large up to about one fourth of the full overlap distance (e.g., 600 m), error in the corrected attenuated backscatter coefficient below this altitude have been addressed using two corrections of the geometrical factor. This has been reported in Figure 7a corresponding to the initial overlap factor and a modified correction profile, corresponding to larger values of the overlap function close to the emission, taking into account a possible error in the O(r) retrieved function. One can see that this significantly modifies values up to 600 m, especially near the surface due to extrapolation, where it can reach +/−50%. Above 600 m, the error is estimated to be less than +/−10%.

[22] In order to more extensively discuss this correction, we have compared these profiles to ceilometer observations acquired at the same period. Starting in mid-January 2006, the Universities of Bonn and Cologne performed continuous remote sensing observations at Djougou using a CT25K Lidar Ceilometer from Vaisala company, modified so to provide vertical backscatter coefficient profiles in the troposphere [*Pospichal and Crewell*, 2007]. The CT25K uses a low-power laser source operating at $\lambda_{Ce}$ = 905 nm to continuously monitor the atmospheric profile. A correction of the overlap function (the 90% overlap range is 300 m) [*Rogers et al.*, 1997] is applied in the Vaisala software. It was providing time height series with a temporal resolution of 15 s and a vertical range of 7500 m (60 m resolution). The profile obtained on 21 January 2006 at the same time than the CAML one is reported in Figure 7b. Both systems show a similar BL depth, determined from the gradient in backscattering [*Dupont et al.*, 1994]. The backscattering by aerosols in the boundary layer is very well observed by the ceilometer down to an altitude very close to the surface, due to a large field of view. This is, however, made to the detriment of range, as this increases noise level. The upper layer aerosol is thus not well detected by the CT25K and the clear air above it is not detected at all. It is to be noted that only relative profile variation with height is considered here, so that absolute CT25K calibration is not an issue.

[23] The signal appears to be rather homogeneous as needed to apply the slope method. The solid line in both Figures 7a and 7b represents the slope of the signal 1/PdP/dr in the boundary layer as given by equation (2). One can see that both slopes, determined from a fit of the logarithmic signals between 400 and 700 m in the BL, are comparable ($-1.2$ $km^{-1}$ for CAML and $-1.1$ $km^{-1}$ for the CT25K at 500 m), but the values near the surface are somewhat different, CAML underestimating the backscatter in the first 300 m, for the modified overlap function. This is not surprising, considering the accuracy of the correction of the geometrical factor, and the extrapolation method used. Assuming a perfectly mixed BL, the slope would correspond to an extinction coefficient of about 0.55–0.6 $km^{-1}$. The BL height obtained would give AODs close to 0.70. On

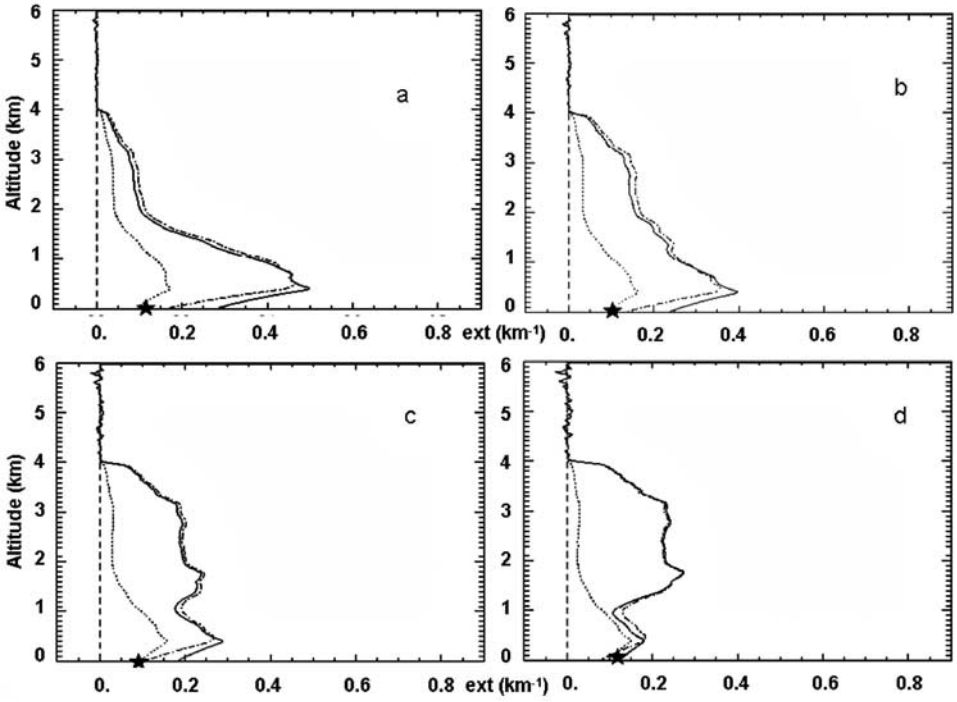


**Figure 8.** Comparison of extinction profiles (solid line) retrieved on 20 January 2006 from Cloud and Aerosol Microlidar (CAML) measurements between 1438 and 1448 LT assuming different lidar ratios in the boundary layer and trade wind layer keeping the total optical depth constant and equal to 0.76. Two overlap corrections are shown initial (*i*, solid line) and modified (*m*, dotted line) for which (a) S1 = S2 = 19(*i*)–22(*m*) $sr^{-1}$, (b) (S1, S2) = (16, 35 $sr^{-1}$)(*i*) and (18, 40 $sr^{-1}$)(*m*), (c) (S1, S2) = (12, 51 $sr^{-1}$) (*i*) and (14, 55 $sr^{-1}$), (d) (S1, S2) = (8, 72 $sr^{-1}$) (*i*) and (10, 70 $sr^{-1}$) (*m*). The star on the *x* axis represents the total extinction coefficient measured by the nephelometer at ground. The separation height is taken equal to 1.2 km. The dotted line represents the attenuated backscattering ratio minus 1 before inversion (same scale without unit).

this day, the total AOD measured by the Sun photometer at 870 nm, which is close to the ceilometer wavelength, is only 0.6 (Figure 2). This implies that the first term in equation (2), representing the inverse scale height of aerosols $\beta^{-1}\mathrm{d}\beta/\mathrm{dr}$, should not be neglected. The use of equation (2) at two wavelengths can help retrieving the extinction, after making a difference to eliminate the backscatter scale height. It also requires to use an additional relationship for the wavelength dependence of the extinction coefficient. Using the spectral wavelength dependence of the extinction involving the Angström exponent A ($\alpha \sim \lambda^{-A}$), allows to write

$$\alpha_{Ca} = \frac{1}{2}\left(\frac{dP_{Ca}}{P_{Ca}dr} - \frac{dP_{Ce}}{P_{Ce}dr}\right)\left(1 - \left(\frac{\lambda_{Ce}}{\lambda_{Ca}}\right)^{-A}\right) \qquad (3)$$

where subscripts Ca and Ce stand for microlidar and ceilometer instruments, respectively. Considering the observations made in the same altitude range by the BAe 146, where we derived an Angström exponent A$\sim$0.5, we find from equation (3) that the extinction at 600 m (at 532 nm) should be about 0.2 $km^{-1}$. This value is slightly higher than what has been measured near the surface, but both values are compatible within the overlap correction error, as will be discussed in section 4.3. Although there is a large uncertainty on this value due to the uncertainty on the slopes, the retrieved value is close to expectations, and the correction using the determined overlap functions (initial and modified) was applied to all profiles.

### 4.3. Derivation of Optical Parameters

[24] Extinction profiles are retrieved from the processing of attenuated backscatter profiles. As two layers are observed from the structural analysis, linked to the very specific dynamics in the region, they may have different optical properties. In the standard approach developed for lidar data inversion, the extinction-to-backscatter ratio (EBR), or lidar ratio, which is the inverse of the normalized aerosol phase function value in the backscattering direction, divided by the aerosol single scattering albedo [*Pelon et al.*, 2002], needs to be known [*Klett*, 1985]. Extinction profiles can be obtained from lidar observations using AODs measured from Sun photometer on a nearby site [*Pelon et al.*, 2002]. Applying a similar procedure, and assuming constant properties on the vertical give the profile reported in Figure 8a for 20 January, in a sequence of 10 min, between 1438 and 1447. Forcing the inversion with an aerosol optical depth of 0.76, allowed to retrieve an EBR value of 19 and 23 sr for the two overlap factor corrections previously defined. These values are smaller than expected for biomass and dust [*Müller et al.*, 2007]. One can see in Figure 8a, that the value of the extinction coefficient measured at the surface is however much smaller that the

**Table 2.** Aerosol Parameters in the Upper Layer Retrieved Over Djougou From Microlidar Observations and Optical Depth From Sun Photometer Used in the Inversion Process

| | 20 Jan 1438–1447 LT | 20 Jan 1714–1723 LT | 21 Jan 1407–1416 LT | 22 Jan 1549–1559 LT | 23 Jan 1246–1255 LT |
|---|---|---|---|---|---|
| S2 (trade wind layer) | 70 | 100 | 130 | 100 | 50 |
| Lidar extinction (at 3 km) ($km^{-1}$) | 0.21 | 0.25 | 0.34 | 0.13 | 0.06 |
| Aerosol optical depth (532 nm) | 0.75 | 0.87 | 0.82 | 0.66 | 0.65 |

retrieved value in both cases (which could be underestimated as previously discussed). The extinction retrieved is also much smaller than observed with the BAe 146 at an altitude of 150 m in the vicinity of Djougou during flight mission B159 made on the previous day (Figure 5). It is however compatible with values observed at 1500 m (Figure 5.), but much smaller than values measured above [*Johnson et al.*, 2008]. In order to adapt the inversion procedure to the change of properties observed both from ground and aircraft, we have looked to use a two-layer inversion approach [*Pelon et al.*, 2002; *Ansmann*, 2006], taking into account the BL height determined from the structural analysis, and inferring a different EBR value in the BL and above to represent the mixing of aerosol type in the boundary layer and size differentiation on the vertical, as evidenced from aircraft observations.

[25] Keeping the same value of the AOD, we looked to the evolution of the extinction profile for various couples of EBRs. Results are reported in Figure 8 for three couples where we considered smaller values of the EBR in the boundary layer and larger above it. We have used a smooth transition over 300 m at the boundary layer top, between the properties of the two layers. The inversion process is controlled by the AOD and the constraint of the surface extinction, which allows to constrain the couple of EBRs. This was done for both correction of the overlap factor.

[26] As seen in Figure 8, this iteration allows to converge toward larger values of the extinction in the upper layer and smaller ones in the lower layer. Unfortunately, no direct comparison could be made, as no flight of the BAe 146 was performed over Djougou during CAML operation. The values obtained however compare qualitatively well with aircraft observations of mission B159, performed on the day before. As reported in Table 2, it was necessary to increase the EBR value in the upper layer to a value of 70 sr. This turns to be close to a standard value for biomass burning aerosols [*Müller et al.*, 2007] and very similar to what has been observed near 12°N at the end of January. (*Heese and Wiegner* [2008] report average values close to 70 sr for biomass burning aerosol observed between 2 and 5 km.) This also led to decrease the EBR in the boundary layer to values of about 10 sr, which are small values as compared to standard results reported in the literature for BL aerosols. However, one should note that the value of the extinction obtained at 600 m (at an altitude where the error due to the overlap factor correction is not too large) is close to the estimation made from comparison with ceilometer data and aircraft. A too small value of EBR means that the backscatter coefficient would be too high in the BL. Despite the good comparisons with ceilometer data in the BL, residual errors could be due to the correction of the geometrical factor below 600 m, and the profile extrapolation to the surface, as well as representativeness of surface measurements used in the iteration process. Error bars on the extinction of about 10% in the upper layer (above 600 m), increasing to the surface to about 50% has been estimated from the analysis performed using two overlap functions. Considering a conservative error value of 50%, on an average extinction coefficient of 0.2 $km^{-1}$ between the surface and a range of 600 m would lead to an error of about 0.06 in optical depth. This represents an error of about 30% of the BL AOD. The impact however remains less than 15% of the residual optical depth due to biomass burning. Comparing these errors to retrieved values shows that the error (positive bias in the upper layer and negative bias in the BL) on EBR values should be of the order of 10 to 20sr. Additional errors may also be due to the undercorrection of afterpulse signal, but tests made did show that they stay between confidence limits.

## 5. Results and Discussion

[27] CAML was operated semiautomatically during the SOP0, and we will focus here on the period of larger occurrence of biomass burning particles as discussed in section 3. Extinction profiles were derived using the previously described procedure up to 6 km for a 10 min acquisition time. Profiles obtained near 1400 LT are reported for the 20 to 23 January in Figure 9 for the initial overlap correction. They show that the extinction in the boundary layer was much less varying than in the upper layer. On 20 January a peak just above the boundary layer was observed, which increased while spreading at upper levels during the night, and led in the following day to an overall increase by a factor of 1.5 of the AOD in the trade wind layer. On 22 January the extinction decreased in this upper layer, but it was seen to dilute toward upper altitudes, as its maximum height increased from 4 to 4.5 km. On 23 January, while this upper limit was maintained with a low extinction in the upper part of the trade wind layer, another peak appeared above the boundary layer top. The profile on 24 January was comparable to the one of 20 January. We have reported in Table 2 the main characteristics of the aerosol layers observed. If the EBR in the boundary layer remains quite similar, the EBR in the trade wind layer, as well as the extinction at an altitude of 3 km is seen to present a maximum value on 21 January, showing than the occurrence of biomass burning aerosol were enhanced on 20 to 21 January.

[28] This corresponds to observations made in M'Bour, where a strong peak in AOD (close to 2) has been recorded on 21 and 22 January, with Angström exponents close to 1.2 [*Derimian et al.*, 2008]. The extinctions retrieved from the lidar data analysis in M'Bour are in the range 0.25–0.3 $km^{-1}$ at a height of 3 km for 21 January, which is comparable to what we retrieved for the Djougou site. It also corresponds to observations made in Niamey-Banizoumbou over the

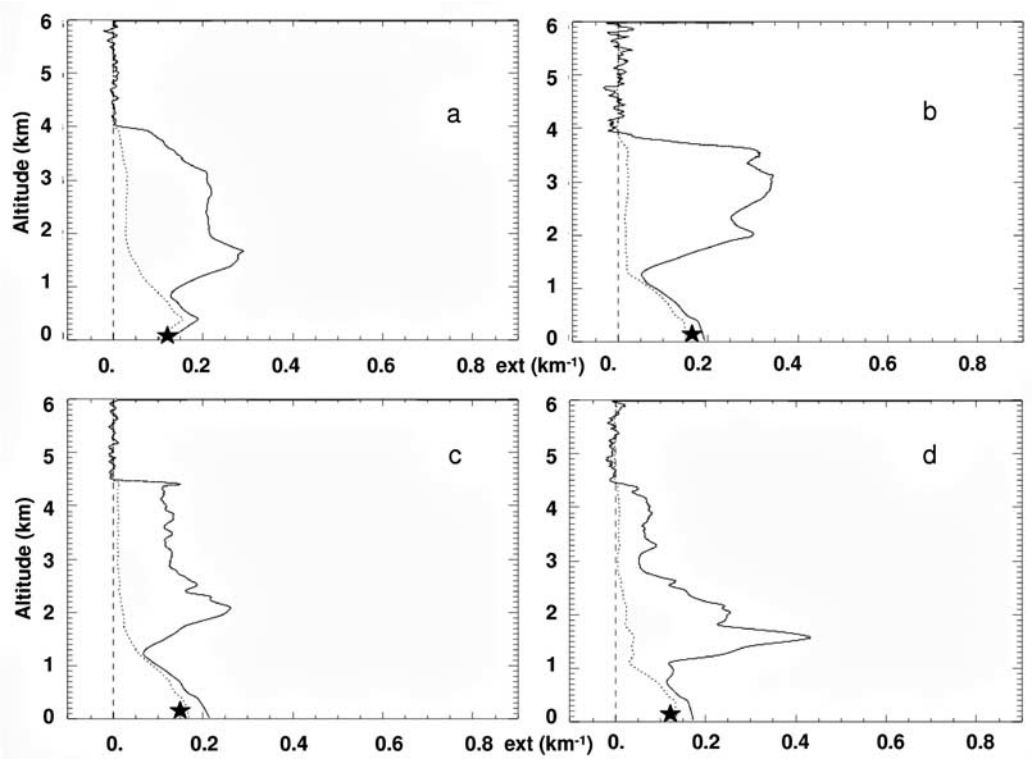


**Figure 9.** Extinction profiles obtained from CAML observations performed on 20 to 23 January 2006. Stars represent the value of the extinction coefficient at the surface. The dotted line represents the attenuated backscattering ratio minus 1 before inversion (same scale without unit).

same period, where large extinctions due to biomass burning aerosols have been recorded by lidar between 1 and 5 km [*Heese and Wiegner*, 2008].

[29] We have looked to satellite data from the AQUA-Train (constellation of 5 satellites in a polar orbit) in order to analyze the extent of air masses. During this period, data have been obtained with the Polarization et Anisotropie des Réflectances au sommet de l'Atmosphère couplées avec un Satellite d'Observation emportant un Lidar (PARASOL) microsatellite. PARASOL is a CNES microsatellite which joined the AQUA-Train in December 2004 [*Tanré et al.*, 2007]. From the ground-based observations, one can see that a large number of small particles of biomass burning origin are present in the trade wind layer, which should lead

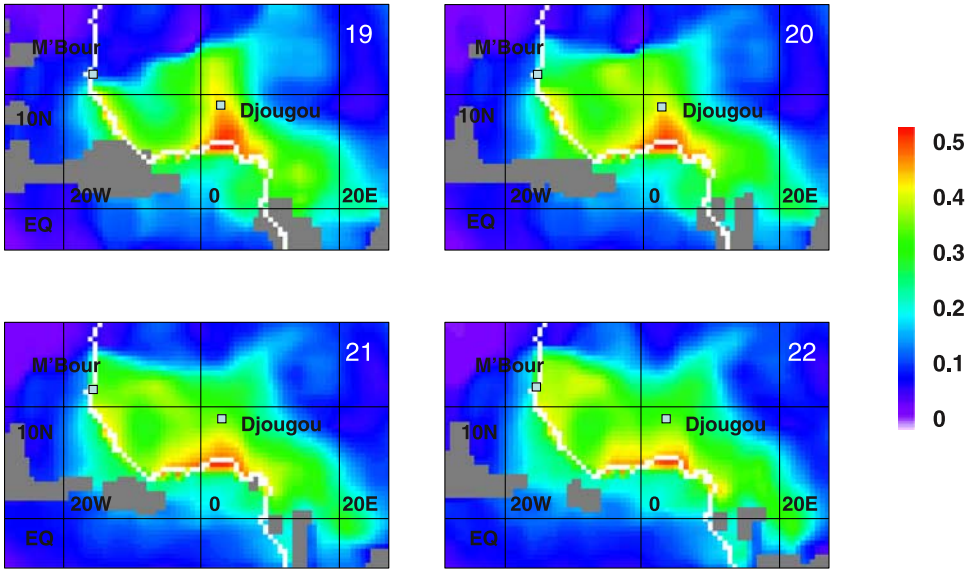


**Figure 10.** Aerosol optical depth in the small mode (less than 0.35 $\mu$m) derived from PARASOL satellite on 19 to 22 January at 670 nm showing a large amount of biomass particles transported to the north of Djougou and then to the west at about 12°N.

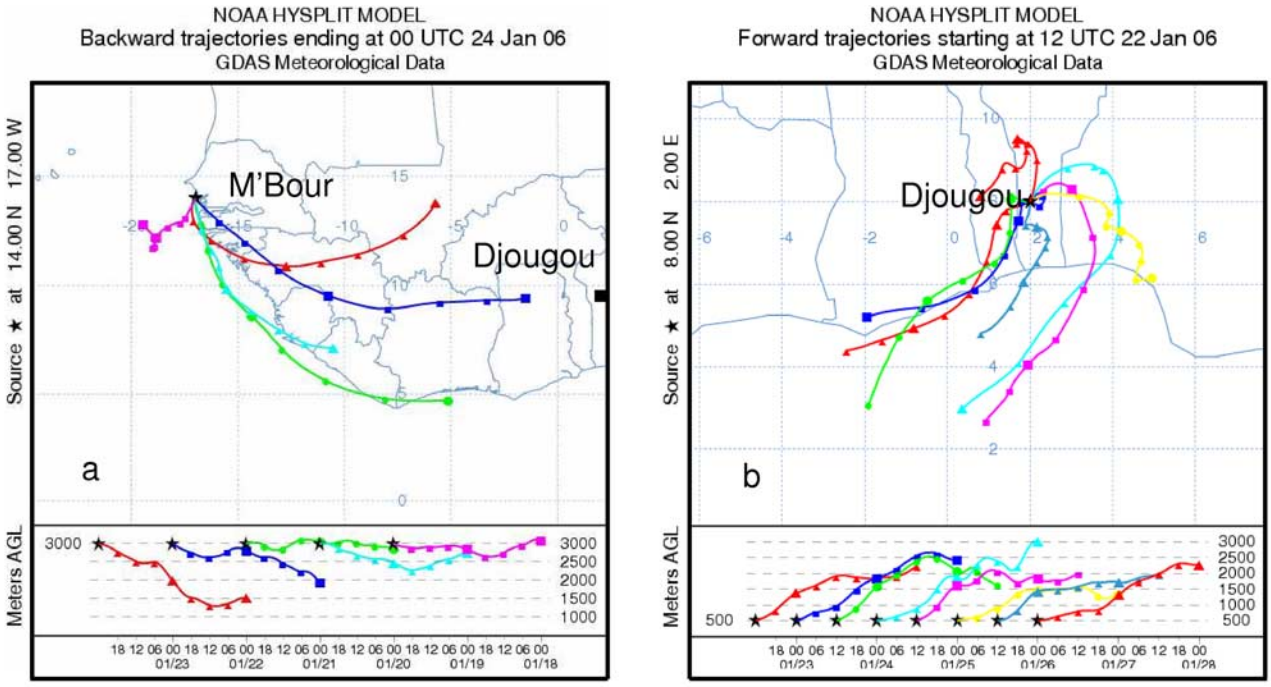


**Figure 11.** (a) Backward trajectories ending at M'Bour (14°N, 17°W) at 3000 m from 20 to 23 January; (b) forward trajectories of biomass burning particles emitted at 8°N, 2°E at 500 m altitude, for the period from 22 to 28 January.

for this event to a large fraction of aerosol identified in the small mode. We have reported in Figure 10 the aerosol optical depth of the small mode obtained for PARASOL for 19 to 22 January period. These data show that Djougou was on 19 January on the edge of a small sized-mode aerosol outflow extending to the north up to 14°N. This outflow was still active on the 20 January and then recessing. On 20 January, part of the air mass has been cut from the outflow and taken into the westerly flow. Its denser part is then located at 8°W on 21 January as some particles seem to reach M'Bour, but the main part of the cutoff air masses arrives on 22 and 23 January.

[30] We have further looked to transport above the BL during the period from 19 to 22 January 2006. Forward trajectories from Djougou at 3 km height and backward trajectories from M'Bour have been made over this period using HYSPLIT trajectory model (http://www.arl.noaa.gov). The backward trajectories reported in Figure 11a show that the particles reaching an altitude of 3 km at M'Bour at the end of the period were coming from the same altitude, as well as from northern latitudes. The forward trajectories show that the air masses originating between 9° and 10°N at 2°W, and located between 2 and 3 km in altitude, are transported to 10°–12°W from 21 to 23 January at constant altitude level. This confirms that PARASOL observations showing preferred north and west trajectories correspond well to elevated layers above the BL.

[31] However, particles reaching M'Bour at the beginning of the event were coming from southern latitudes, e.g., closer to the south of the coast (south of Côte d'Ivoire). The increase in extinction observed in M'Bour on 21 January (turquoise blue back-trajectory in Figure 11) is thus not due to the event observed in Djougou but to the transport of biomass burning air masses from elevated layers over Liberia close to the coast.

[32] The whole trade wind layer south of 10°N should thus be filled with biomass burning aerosols produced at the surface. To check this, we have further looked at forward trajectories of particles emitted close to the Djougou observation site from a point located at 8°N, 0°W, in the boundary layer at 500 m altitude, for different days over the same period of January. From trajectories plotted in Figure 11b, it is interesting to note that the particles are all transported to upper levels above the BLH in about 2 days and are then transported to the south, leading to an accumulation of particles over the ocean. This is confirmed by space observations (Figure 12), although one should consider that errors on values over land are larger [*Remer et al.*, 2005]. Values reported here over Djougou appear smaller that those for photometer measurements. The vertical transport from the BL to the trade wind layer is most probably due to the dynamics of the monsoon flow. Indeed during the summer period, the monsoon flow has been analyzed when the ITD reaches the dust hot spots, using aircraft observations and mesoscale modeling. It was shown that the dynamics of the monsoon current could lead to an efficiently transport of dust above the BL due to strong turbulence, near and behind the ITD [*Bou Karam et al.*, 2008]. We think similar processes can take place during the dry season and lead to the vertical transport of biomass as the ITD steadily progresses but also oscillates on a day-to-day basis.

[33] MODIS AODs averaged over the period from 18 to 24 January 2006 confirm the existence of an accumulation of aerosol particles over the ocean, leading to a large optical depth south of 5°N. The accumulation of biomass burning particles in altitude south of 10°N is also evidenced by

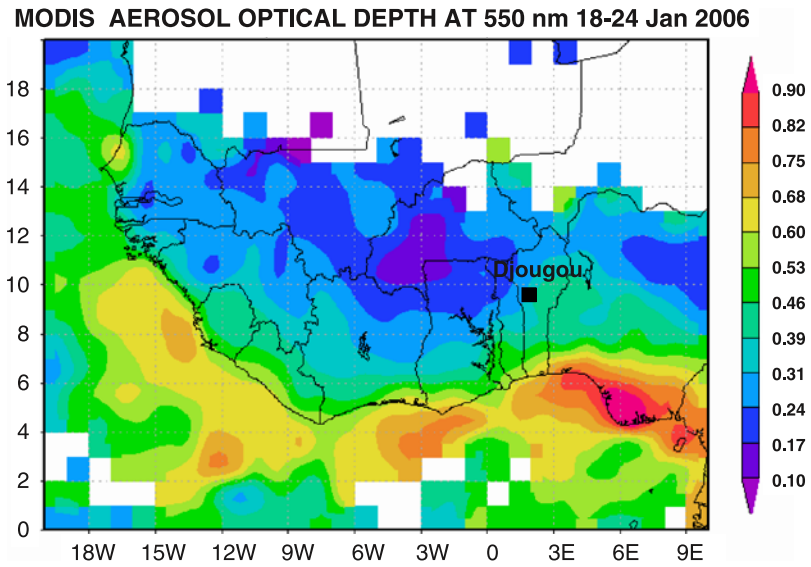


**Figure 12.** MODIS average AOD for the period from 18 to 24 January showing maximal values over the ocean.

LMDZ-INCA simulations [*Schulz et al.*, 2006], performed in forecast mode during the SOP 0, by Laboratoire des Sciences du Climat et de l'Environnement (LSCE/IPSL). These data are archived in the AMMA database.

[34] From these observations, we can conclude that particles should thus be transported in a two-step process. A first step is to transport biomass from the BL to the trade wind layer close at the head of the monsoon flow (ITD area), and a second one to transport the particles to the south and redistribute it regionally, preferentially close to the ITCZ. The proposed scheme is presented in the introduction paper (Haywood et al., submitted manuscript, 2008). The transport event observed here during several days in the period 19 to 23 January may have led to a significant depletion of the aerosol reservoir over the south of the continent. The aerosol outbreak to the north during this event is likely to be associated with a synoptic forcing due to the position of the low over northern Africa, leading to a descent in latitude of the subtropical jet, coupling midlevel and high-level circulations, and forcing air mass transport to the north, e.g., opposite of the average circulation.

## 6. Conclusion

[35] Microlidar measurements performed in Djougou during the AMMA-SOP0/DABEX campaign held during the dry season have been analyzed to characterize aerosol properties, in January and February 2006. During this first intensive observing period of AMMA, lidar observations performed on a quasi-continuous basis have led to building a database which will be used for further studies. We have made here a first analysis of such data. Taking advantage in the synergism between ground-based instruments installed in Djougou, a new method was developed and tested to characterize aerosol properties in a two-layer structure on the vertical. It was shown that large quantities of biomass burning aerosols were transported in the trade wind layer above the boundary layer. Most of them appear to be advected over the ocean, where they could accumulate. Characterization of aerosols was more particularly performed during a special biomass burning outbreak event. This transport to the north was most probably linked to the undulation of the subtropical jet stream due to the deepening of a low over northern Algeria and its eastward motion. This type of event led to an unusual transport to the north of biomass burning particles, which was observed by the PARASOL satellite and ground-based stations. Further mesoscale model analyses need to be performed to address this question as well as the accumulation of biomass burning aerosols and their radiative impact at the regional scale.

[36] **Acknowledgments.** On the basis of a French initiative, AMMA was built by an international scientific group and is currently funded a large number of agencies especially from France, UK, United States, and Africa. It has been the beneficiary of a major financial contribution from the European Community's Sixth Framework Research Programme. Detailed information on scientific coordination is available on the AMMA international Web site (http://www.amma-international.org). Particular thanks go to L. Blarel (LOA), who installed the CIMEL station in Djougou, T. Podvin (LOA) for providing M'Bour CAML data, and P. Genau (SA) for his help in data processing.

## References

Andreae, M., and P. Merlet (2001), Emission of trace gases and aerosols from biomass burning, *Global Biogeochem. Cycles*, *15*(4), 955–966, doi:10.1029/2000GB001382.

Ansmann, A. (2006), Ground-truth aerosol lidar observations: Can the Klett solutions obtained from ground and space be equal for the same aerosol case?, *Appl. Opt.*, *45*(14), 3367–3371, doi:10.1364/AO.45.003367.

Berthier, S., P. Chazette, P. Couvert, J. Pelon, F. Dulac, F. Thieuleux, C. Moulin, and T. Pain (2006), Desert dust aerosol columnar properties over ocean and continental Africa from Lidar in-Space Technology Experiment (LITE) and Meteosat synergy, *J. Geophys. Res.*, *111*, D21202, doi:10.1029/2005JD006999.

Bou Karam, D., C. Flamant, P. Knippertz, O. Reitebuch, J. Pelon, M. Chong, and A. Dabas (2008), Dust emissions over Sahel associated with the West African Monsoon inter-tropical discontinuity region: A representative case study, *Q. J. R. Meteorol. Soc.*, *134*, 621–634.

d'Almeida, G. A. (1986), A model for Saharan dust transport, *J. Clim. Appl. Meteorol.*, *25*, 903–916, doi:10.1175/1520-0450(1986)025<0903:AMFSDT>2.0.CO;2.

Derimian, Y., J.-F. Leon, O. Dubovik, I. Chiapello, D. Tanré, A. Sinyuk, F. Auriol, T. Podvin, G. Brogniez, and B. N. Holben (2008), Radiative properties of aerosol mixing observed over M'Bour in Senegal during the dry season 2006 (African Monsoon Multidisciplinary Analysis campaign), *J. Geophys. Res.*, *113*, D00C09, doi:10.1029/2008JD009904.

Dupont, E., J. Pelon, and C. Flamant (1994), Study of the moist convective atmospheric boundary layer structure by backscatter lidar, *Boundary Layer Meteorol.*, *69*, 1–25, doi:10.1007/BF00713292.

Flamant, C., and J. Pelon (1996), Atmospheric boundary-layer structure over the Mediterranean during a Tramontane event, *Q. J. R. Meteorol. Soc.*, *122*, 1741–1778, doi:10.1256/smsqj.53601.

Fraser, R. S., and Y. J. Kaufman (1985), The relative importance of scattering and absorption in remote sensing, *IEEE Trans. Geosci. Remote Sens.*, *23*, 625–633, doi:10.1109/TGRS.1985.289380.

Haywood, J. M., S. R. Osborne, P. N. Francis, A. Keil, P. Formenti, M. O. Andreae, and P. H. Kaye (2003), The mean physical and optical properties of regional haze dominated by biomass burning aerosol measured from the C-130 aircraft during SAFARI 2000, *J. Geophys. Res.*, *108*(D13), 8473, doi:10.1029/2002JD002226.

Heese, B., and M. Wiegner (2008), Vertical aerosol profiles from Raman-depolarization lidar observations during the dry season AMMA field campaign, *J. Geophys. Res.*, *113*, D00C11, doi:10.1029/2007JD009487.

Husar, R. B., J. M. Prospero, and L. L. Stowe (1997), Characterization of tropospheric aerosols over the oceans with the NOAA advanced very high resolution radiometer optical thickness operational product, *J. Geophys. Res.*, *102*, 16,889–16,909, doi:10.1029/96JD04009.

Johnson, B. T., S. R. Osborne, and J. M. Haywood (2008), Aircraft measurements of biomass-burning aerosols over West Africa during DABEX, *J. Geophys. Res.*, *113*, D00C06, doi:10.1029/2007JD009451.

Karyampudi, V. M., et al. (1999), Validation of the Saharan Dust Plume Conceptual Model using lidar, Meteosat, and ECMWF data, *Bull. Am. Meteorol. Soc.*, *80*(6), 1045–1075.

Kaufman, Y. J., D. Tanré, J.-F. Léon, and J. Pelon (2003), Retrievals of profiles of fine and coarse aerosols using lidar and radiometric space measurements, *IEEE Trans. Geosci. Remote Sens.*, *41*, 1743–1754.

Klett, J. D. (1985), Lidar inversion with variable backscatter/extinction ratios, *Appl. Opt.*, *24*, 1638–1643.

Kunz, G. J., and G. de Leeuw (1993), Inversion of lidar signals with the slope method, *Appl. Opt.*, *32*, 3249.

Mallet, M., et al. (2008), Aerosol direct radiative forcing over Djougou (northern Benin) during the African Monsoon Multidisciplinary Analysis dry season experiment (Special Observation Period-0), *J. Geophys. Res.*, *113*, D00C01, doi:10.1029/2007JD009419.

Menut, L., C. Flamant, J. Pelon, and P. H. Flamant (1999), Urban boundary layer height determination from lidar measurements over the Paris area, *Appl. Opt.*, *38*(6), 945–954, doi:10.1364/AO.38.000945.

Müller, D., A. Ansmann, I. Mattis, M. Tesche, U. Wandinger, D. Althausen, and G. Pisani (2007), Aerosol-type-dependent lidar ratios observed with Raman lidar, *J. Geophys. Res.*, *112*, D16202, doi:10.1029/2006JD008292.

O'Neill, N. T., T. F. Eck, B. N. Holben, A. Smirnov, A. Royer, and Z. Li (2002), Optical properties of boreal forest fire smoke derived from Sun photometry, *J. Geophys. Res.*, *107*(D11),4125,doi:10.1029/2001JD000877.

Parker, D. J., R. R. Burton, A. Diongue-Niang, R. J. Ellis, M. Felton, C. M. Taylor, C. D. Thorncroft, P. Bessemoulin, and A. M. Tompkins (2005), The diurnal cycle of the west African monsoon circulation, *Q. J. R. Meteorol. Soc.*, *131*, 2839–2860, doi:10.1256/qj.04.52.

Pelon, J., C. Flamant, P. Chazette, J.-F. Léon, D. Tanré, M. Sicard, and S. K. Satheesh (2002), Characterization of aerosol spatial distribution and optical properties over the Indian Ocean from airborne lidar and radiometry during INDOEX'99, *J. Geophys. Res.*, *107*(D19), 8029, doi:10.1029/2001JD000402.

Pospichal, B., and S. Crewell (2007), Boundary layer observations in West Africa using a novel microwave radiometer, *Meteorol. Z.*, *16*(5), 513–523, doi:10.1127/0941-2948/2007/0228.

Prospero, J. M., P. Ginoux, O. Torres, S. E. Nicholson, and T. E. Gill (2002), Environmental characterization of global sources of atmospheric dust identified with the nimbus 7 Total Ozone Mapping Spectrometer (TOMS) absorbing aerosols product, *Rev. Geophys.*, *40*(1), 1002, doi:10.1029/2000RG000095.

Ramel, R., H. Gallée, and C. Messager (2006), On the northward shift of the West African monsoon, *Clim. Dyn.*, *26*(4), 429–440, doi:10.1007/s00382-005-0093-5.

Remer, L. A., et al. (2005), The MODIS aerosol algorithm, products and validation, *J. Atmos. Sci.*, *62*, 947–973, doi:10.1175/JAS3385.1.

Rogers, R. R., L. R. Bissonnette, and R. M. Peters (1997), Quantitative interpretation of laser ceilometer intensity profiles, *J. Atmos. Oceanic Technol.*, *14*, 396–411, doi:10.1175/1520-0426(1997)014<0396:QIOLCI>2.0.CO;2.

Schulz, M., et al. (2006), Radiative forcing by aerosols as derived from the AeroCom, present-day and pre-industrial simulations, *Atmos. Chem. Phys.*, *6*, 5225–5246.

Tanré, D., J. M. Haywood, J. Pelon, J. F. Léon, B. Chatenet, P. Formenti, P. Francis, P. Goloub, E. J. Highwood, and G. Myhre (2003), Measurement and modeling of the Saharan dust radiative impact: Overview of the Saharan Dust Experiment (SHADE), *J. Geophys. Res.*, *108*(D18), 8574, doi:10.1029/2002JD003273.

Tanré, D., et al. (2007), Aerosol remote sensing from the PARASOL mission and the A-train, paper presented at First A-Train Symposium, Centre Natl. d'Etud. Spatiales, Lille, France.

Tulet, P., M. Mallet, V. Pont, J. Pelon, and A. Boone (2008), The 7–13 March dust storm over West Africa: Generation, transport and vertical stratification, *J. Geophys. Res.*, *113*, D00C08, doi:10.1029/2008JD009871.

Welton, E. J., K. J. Voss, P. K. Quinn, P. J. Flatau, K. Markowicz, J. R. Campbell, J. D. Spinhirne, H. R. Gordon, and J. E. Johnson (2002), Measurements of aerosol vertical profiles and optical properties during INDOEX 1999 using micropulse lidars, *J. Geophys. Res.*, *107*(D19), 8019, doi:10.1029/2000JD000038.

D. Bou Karam, C. Flamant, and J. Pelon, SA, UPMC, IPSL, CNRS, B102, 4, Place Jussieu, F-75252 Paris CEDEX 05, France. (jpe@aero.jussieu.fr)

P. Goloub and D. Tanré, LOA, Université Lille 1, CNRS, P5, F-59655 Villeneuve d'Asq, France.

J. Haywood, Met Office, FitzRoy Road, Exeter EX1 3PB, UK.

M. Mallet and A. Mariscal, LA, UPS, CNRS, 14, av. Belin, F-31400 Toulouse, France.

B. Pospichal, Institute for Geophysics and Meteorology, University of Cologne, Kerpener Str. 13, D-50923 Köln, Germany.

S. Victori, CIMEL Electronique, F-75011 Paris, France.